



Triaxial Creep Behaviour of Limestone under Graded Confining Pressure Unloading



Boning Zhang^{ID}, Shiwei Shen^{*}^{ID}

College of Construction Engineering, Jilin University, 130026 Jilin, China

* Correspondence: Shiwei Shen (ssw2580@jlu.edu.cn)

Received: 07-09-2024

Revised: 08-19-2024

Accepted: 09-05-2024

Citation: B. N. Zhang and S. W. Shen, "Triaxial creep behaviour of limestone under graded confining pressure unloading," *GeoStruct. Innov.*, vol. 2, no. 3, pp. 117–124, 2024. <https://doi.org/10.56578/gsi020301>.



© 2024 by the author(s). Published by Acadlore Publishing Services Limited, Hong Kong. This article is available for free download and can be reused and cited, provided that the original published version is credited, under the CC BY 4.0 license.

Abstract: The stability of rock masses in large-scale hydropower projects and high-slope excavation engineering is significantly influenced by the unloading of confining pressure. This study investigates the triaxial creep behaviour of limestone under varying conditions of confining pressure unloading through systematic experimental research. Using a ZYSS2000C triaxial shear rheometer, limestone samples from the Qinling region were subjected to a series of triaxial creep tests with controlled unloading conditions. Experimental setups included varying single-step unloading magnitudes of confining pressure (2 MPa, 4 MPa, and 6 MPa) under constant axial stress. The results demonstrated that the magnitude of confining pressure unloading had a pronounced impact on creep behaviour. Larger unloading magnitudes led to shorter total creep durations and reduced cumulative deformation, highlighting the pivotal role of unloading intensity in governing creep characteristics. During the unloading creep process, the deviatoric stress of the rock decreased, and the deformation predominantly manifested as radial dilation. These findings provide new insights into the rock deformation mechanisms induced by confining pressure unloading and offer valuable theoretical and practical guidance for slope excavation and stability management.

Keywords: Triaxial creep; Unloading; Limestone

1 Introduction

Rock masses on high slopes are typically in a relatively stable tri-axial stress state under natural conditions. However, excavation-induced disturbances can lead to stress redistribution in the region, resulting in unloading deformation of the rock masses [1–5]. Although slope structures under the newly adjusted stress state may not experience immediate instability, long-term creep deformation can eventually cause slope failure [6–8]. Such failures, including slope collapses, can lead to catastrophic consequences when they occur [9]. To mitigate the risks posed by these hazards to dam structures, it is crucial to conduct in-depth investigations into the creep deformation patterns and mechanical characteristics of hard rock under varying axial stresses and confining pressure unloading magnitudes. Examining the triaxial unloading creep behaviour of rocks using stress paths that closely mimic real-world excavation scenarios holds significant scientific and engineering value.

The mechanical properties of hard rock under unloading conditions differ markedly from those observed during loading. Unloading not only significantly reduces the strength of rock masses and induces unloading softening but also results in fewer fractures and lower deformation magnitudes in brittle hard rocks compared to soft rocks. Furthermore, unloading creep exhibits more pronounced lateral dilation when compared to loading creep [10, 11]. Unloading also causes greater disturbance to intact rock, leading to notable reductions in mechanical parameters of rocks due to variations in yield conditions, long-term strength, and loading conditions [12–14].

Despite ongoing research, the impact of confining pressure unloading on rock creep under triaxial stress conditions remains insufficiently explored. Zhao and Jiang [15] conducted triaxial unloading creep experiments on deep sandstone under varying initial stress and hydraulic pressure conditions, revealing the mechanical behaviour and time-dependent deformation characteristics of rock masses under high stress and high water pressure. Yan et al. [16] investigated the basalt foundation of the Baihetan Hydropower Station through triaxial unloading creep tests and established an exponential relationship between confining pressure and steady-state creep rates. Yan et al. [17] conducted triaxial compression gradient unloading creep experiments on the flint limestone from the underground cavern of the Shuibuya Hydropower Station, following the stress paths encountered in real engineering projects.

It was observed that higher unloading magnitudes resulted in reduced ultimate creep failure strength and induced varying failure modes. Zhang et al. [18] studied the creep failure mechanisms of granite under true triaxial unloading conditions. The findings indicated that unloading of σ_3 caused the dilation of ε_v ; ε_2 was not sensitive to the unloading of σ_3 , but ε_3 was very sensitive to the unloading of σ_3 . Existing studies predominantly focus on the influence of unloading behaviour on rock creep patterns. However, investigations simulating excavation-induced stress changes and in-depth exploring the effects of varying unloading magnitudes on rock creep remain rare [19–21].

Building on previous research, this study employed the ZYSS2000C triaxial shear rheometer to conduct triaxial unloading creep experiments on limestone from the Qinling region under varying axial stress conditions. The creep deformation and failure patterns of rock samples were determined under different unloading magnitudes.

2 Sample Preparation and Experimental Methodology

2.1 Sample Preparation

The limestone samples used in this study were sourced from an engineering site in the Qinling Mountains, China. The limestone exhibited a uniform grey-white appearance, with calcite as the predominant mineral composition. The density of the material ranged between 2.62 g/cm^3 to 2.76 g/cm^3 . Cylindrical specimens with a diameter of 50 mm and a height of 100 mm were prepared in accordance with standard protocols. The P-wave velocity of the specimens was measured, with values ranging from 5,012 m/s to 5,635 m/s. Figure 1 shows the photograph of the prepared specimens. Figure 2 shows the photograph of the ultrasonic testing equipment.



Figure 1. Prepared specimens



Figure 2. Ultrasonic testing equipment



Figure 3. Triaxial shear rheometer

2.2 Experimental Scheme

To minimise errors arising from the inherent variability of natural rock samples and to obtain more comprehensive mechanical parameters from individual specimens, a graded unloading approach was adopted. Considering practical engineering conditions, the stress path employed in this study involved constant axial stress combined with graded unloading of the confining pressure. For each stress path, three experiments were conducted to ensure reliability. Prior to the formal tests, essential mechanical parameters were determined through uniaxial compression and triaxial compression experiments. Based on the in-situ stress conditions at the sampling location, an initial confining pressure of 24 MPa was selected for the triaxial unloading creep tests. To simulate actual excavation scenarios, three confining pressure unloading increments ($\Delta\sigma_3$) were defined: 2 MPa, 4 MPa, and 6 MPa. Results from triaxial compression experiments indicated that the peak stress (σ_f) of the samples at a confining pressure of 24 MPa was 246.155 MPa, with crack initiation stress (σ_{ci}) at 124.17 MPa and dilation stress (σ_{cd}) at 177.94 MPa. Axial stress levels were determined as 60% σ_f (148 MPa), 70% σ_f (172 MPa), and 80% σ_f (196 MPa) of the peak stress. Figure 3 shows the photograph of the triaxial shear rheometer.

The experiments were conducted using a ZYSS2000C triaxial shear rheometer developed by China Machine Test Equipment Co., Ltd.

The confining pressure and axial stress were initially applied at a loading rate of 0.05 MPa/s until both reached 24 MPa. Once stress and deformation stabilisation were achieved, the axial stress (σ_1) was further increased at a rate of 0.2 MPa/s to predetermined levels of 148 MPa, 172 MPa, and 196 MPa. These axial stress levels were then maintained constant throughout the unloading process. With 24 MPa as the initial confining pressure (σ_3), graded unloading increments ($\Delta\sigma_3$) were 2 MPa, 4 MPa, and 6 MPa. At each unloading step, deformation stabilisation was ensured ($d\varepsilon/dt \leq 5 \times 10^{-5} h^{-1}$), before proceeding to the next unloading step. The process continued until the specimen reached failure.

3 Results and Analysis

3.1 Time-Strain Relationship Analysis

The overall creep deformation behaviour of the specimens exhibited generality, characterised by instantaneous deformation during initial unloading stages, followed by primary decelerating creep, secondary steady-state creep, and a pronounced accelerated creep stage during failure. It was observed that the strain rate of the creep increased significantly and rapidly as failure approached.

A comparison of axial and radial deformation curves revealed distinct differences from loading experiments. After confining pressure unloading, the radial creep deformation showed a considerably larger increase, highlighting a pronounced radial dilation effect. Furthermore, during each unloading step, the incremental radial instantaneous strain was greater than the corresponding axial instantaneous strain increment. Figure 4 shows the time-strain curves under an axial stress of 148 MPa.

3.2 Deviatoric Stress-Strain Relationship Analysis

Figure 5 shows the deviatoric stress-strain curves for triaxial unloading creep. During the compression stage of axial stress loading, the radial strain of the specimen was found to be only 14.6% to 36.8% of the axial strain. At this stage, the specimen was subjected to triaxial compression, where axial stress (σ_1) primarily contributed to the overall deformation of the specimen, mainly manifested as axial compression deformation. In the subsequent stage,

with axial stress held constant and confining pressure gradually unloaded, the specimen experienced a reduction in σ_3 . This reduction was equivalent to the application of tensile stress in the lateral direction of the specimen, and the radial expansion deformation caused by confining pressure unloading played a dominant role in the overall deformation of the specimen. By the time of specimen failure, the radial strain had increased to 69.7%–103.1% of the axial strain.

The influence of single-step unloading magnitudes on specimen strain during confining pressure unloading and creep was significant. Under identical axial stress levels, larger unloading magnitudes resulted in lower total strain and reduced deviatoric stress at the point of failure. The reduction in confining pressure decreased the lateral restraint on the specimen, leading to increased strain with the rise in deviatoric stress.

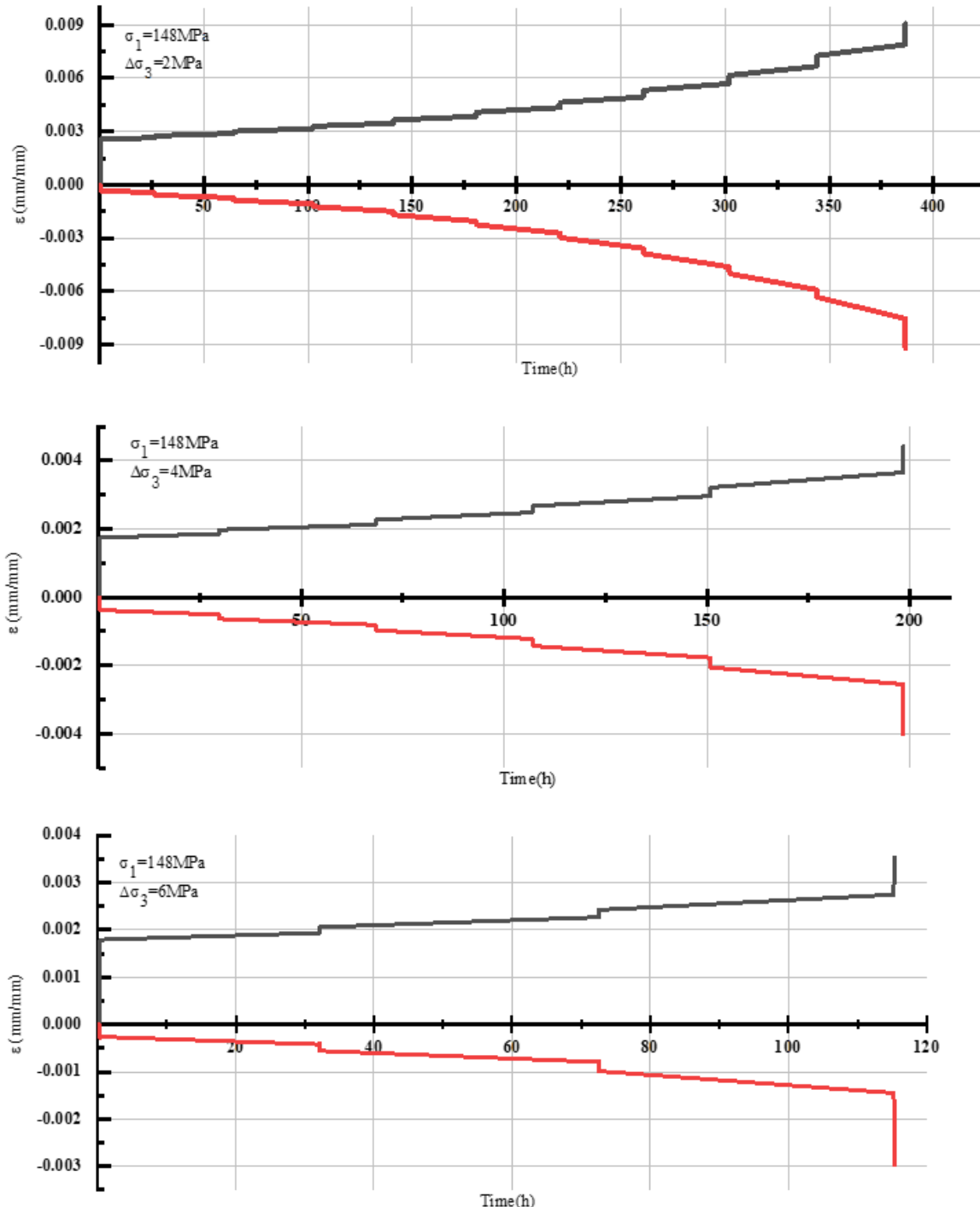


Figure 4. Time-strain curves under an axial stress of 148 MPa

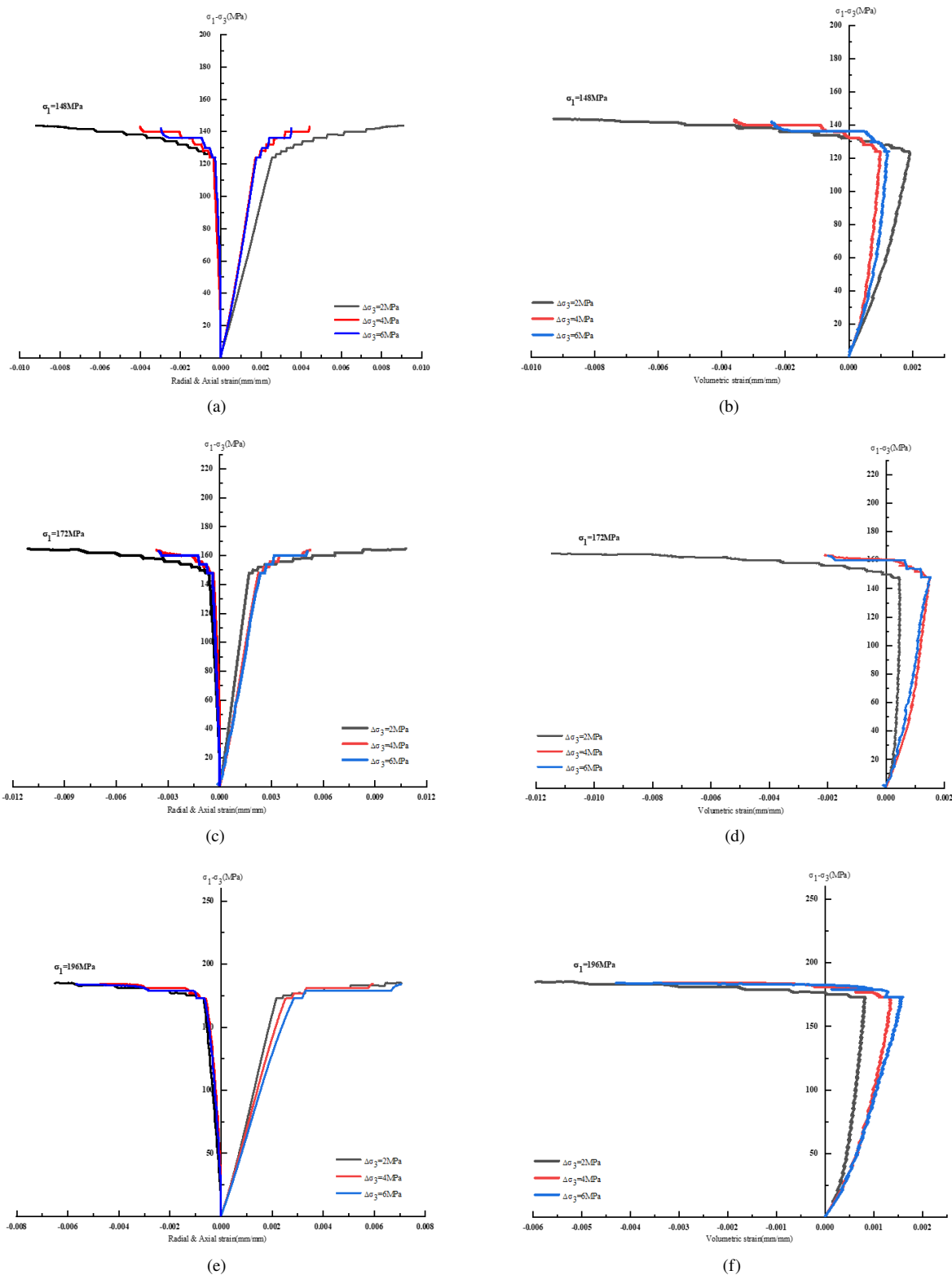


Figure 5. Deviatoric stress-strain curves for triaxial unloading creep: (a) Deviatoric stress vs. axial and radial strain under an axial stress of 148 MPa; (b) Deviatoric stress vs. volumetric strain under a deviatoric stress of 148 MPa; (c) Deviatoric stress vs. axial and radial strain under an axial stress of 172 MPa; (d) Deviatoric stress vs. volumetric strain under a deviatoric stress of 172 MPa; (e) Deviatoric stress vs. axial and radial strain under an axial stress of 196 MPa; (f) Deviatoric stress vs. volumetric strain under a deviatoric stress of 196 MPa

3.3 Deformation Patterns of Unloading Creep

The creep deformation of rock under triaxial unloading conditions is influenced by both axial stress and the magnitude of single-step unloading of confining pressure, and this influence follows distinct patterns. Figure 6 shows the comparison of unloading creep strain under different axial stresses with a single-step unloading magnitude of 2 MPa.

When the magnitude of single-step unloading of confining pressure remains constant, the creep deformation increases with rising axial stress. As shown in Figure 6, under identical conditions, greater axial stress leads to larger creep deformation. Additionally, the increment in creep deformation per unloading step under 60% σ_f axial stress was noticeably smaller compared to that observed under the other two axial stress levels. This phenomenon can be attributed to the transition of axial stress from 60% σ_f to 70% σ_f , corresponding to the transition from crack initiation stress to dilation stress. Within this range, the internal cracks of the specimen become more developed, leading to more pronounced strain changes.

Figure 7 shows the comparison of unloading creep strain under different single-step unloading magnitudes at an axial stress of 172 MPa. When axial stress is held constant, the number of unloading steps required to reach the same reduction in confining pressure increases as the magnitude of single-step unloading decreases. Under such conditions, the cumulative creep deformation of the specimen becomes greater. Conversely, for each individual unloading step, larger unloading magnitudes result in greater creep deformation.

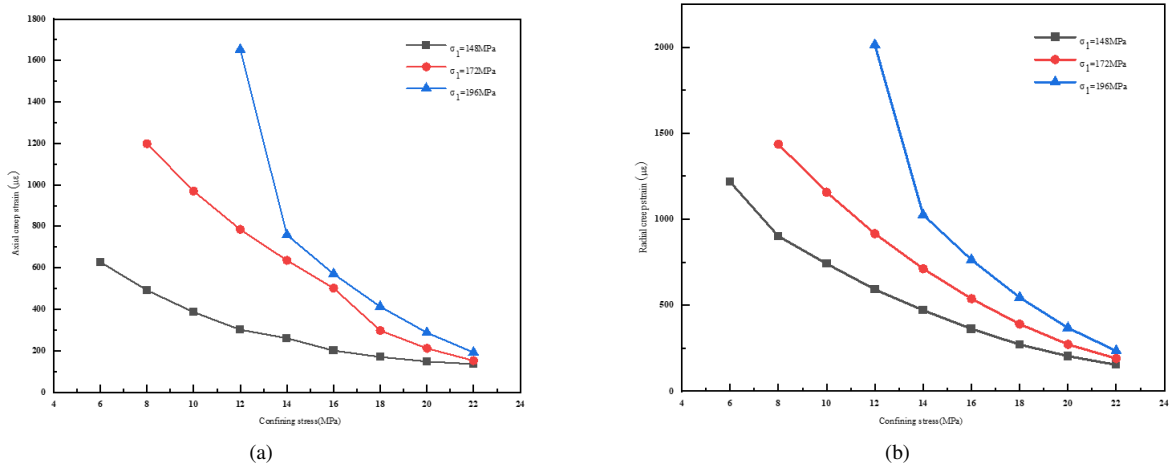


Figure 6. Comparison of unloading creep strain under different axial stresses with a single-step unloading magnitude of 2 MPa: (a) Confining pressure vs. axial strain; (b) Confining pressure vs. volumetric strain

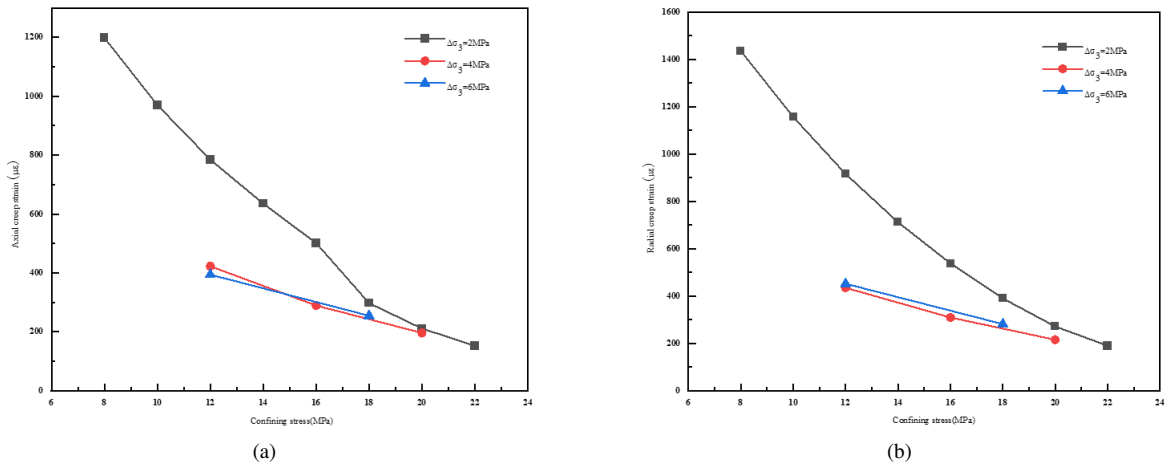


Figure 7. Comparison of unloading creep strain under different single-step unloading magnitudes at an axial stress of 172 MPa: (a) Confining pressure vs. axial strain; (b) Confining pressure vs. volumetric strain

Table 1. Fracture angles under different experimental conditions

σ_1 (MPa)	148				172				196			
$\Delta\sigma_3$ (MPa)	2	4	6	2	4	6	2	4	6	4	6	
Fracture angle θ (°)	55	68	74	48	58	62	69	75	81			

3.4 Failure Characteristics of Unloading Creep

The specimens subjected to triaxial unloading creep tests exhibited failure modes characteristic of tensile-shear failure. The fracture angles under various experimental conditions are presented in Table 1. It was observed that variations in single-step unloading magnitude significantly influenced the fracture angle. As the unloading magnitude increased, the fracture angle also increased noticeably.

When the axial stress was 148 MPa (60% σ_f), the fracture surfaces displayed distinct inclined dislocation. Numerous microcracks were observed around the fracture surfaces, and the specimen exhibited significant volumetric dilation. At an axial stress of 172 MPa (70% σ_f), the fractures were less penetrative, and overall volumetric dilation was not prominent, though localised dilation was evident in certain regions. Under an axial stress of 196 MPa (80% σ_f), the failure mode transitioned to apparent brittle failure, accompanied by chipping at the specimen's ends.

4 Conclusion

The triaxial creep experiments involving confining pressure unloading on limestone from the Qinling region revealed the significant influence of unloading on the creep behaviour of limestone. The experimental results demonstrated that as the magnitude of single-step unloading increased, total creep deformation decreased, and creep duration was shortened. These findings provide critical insights into the deformation behaviour of rock masses under practical engineering conditions. The study further identified that shear failure was the predominant failure mode during unloading, and larger single-step unloading magnitudes were associated with greater impacts on the long-term stability of rock masses. These conclusions offer valuable guidance for the design of safe and effective slope excavation strategies. It is recommended that future research explore the behavioural differences of various rock types under similar unloading conditions and examine the influence of unloading rates on creep characteristics. Additionally, the adoption of moderate unloading measures in engineering practice is advised to mitigate the risk of rock mass failure caused by rapid unloading and to ensure the long-term stability of engineering projects.

Author Contributions

Shiwei Shen, writing – review & editing, supervision; Boning Zhang, writing–original draft, data analysis, experiment, and data collection.

Data Availability

The data used to support the research findings are available from the corresponding author upon request.

Conflicts of Interest

The authors declare no conflict of interest.

References

- [1] T. Szwedzicki, “Rock mass behaviour prior to failure,” *Int. J. Rock Mech. Min. Sci.*, vol. 40, no. 4, pp. 573–584, 2003. [https://doi.org/10.1016/s1365-1609\(03\)00023-6](https://doi.org/10.1016/s1365-1609(03)00023-6)
- [2] A. Singh, C. Kumar, L. G. Kannan, K. S. Rao, and R. Ayothiraman, “Estimation of creep parameters of rock salt from uniaxial compression tests,” *Int. J. Rock Mech. Min. Sci.*, vol. 107, pp. 243–248, 2018. <https://doi.org/10.1016/j.ijrmms.2018.04.037>
- [3] J. C. Innocente, C. Paraskevopoulou, and M. S. Diederichs, “Estimating the long-term strength and time-to-failure of brittle rocks from laboratory testing,” *Int. J. Rock Mech. Min. Sci.*, vol. 147, 2021. <https://doi.org/10.1016/j.ijrmms.2021.104900>
- [4] O. Hamza and R. Stace, “Creep properties of intact and fractured muddy siltstone,” *Int. J. Rock Mech. Min. Sci.*, vol. 106, pp. 109–116, 2018. <https://doi.org/10.1016/j.ijrmms.2018.03.006>
- [5] P. Y. Yu, P. Z. Pan, G. L. Feng, Z. F. Wang, and S. T. Miao, “The effect of unloading path on the time-dependent behavior of Beishan granite,” *Lithosphere*, vol. 2022, no. Special 11, p. 3112805, 2022. <https://doi.org/10.2113/2022/3112805>

- [6] W. D. Yang, X. P. Wang, N. Liu, and Q. Wang, “An analytical solution for the time-dependent anchoring force in prestressed cables due to rock creep,” *Mech. Time-Depend. Mater.*, vol. 27, no. 2, pp. 367–399, 2023. <https://doi.org/10.1007/s11043-022-09577-6>
- [7] E. Kabwe, M. Karakus, and E. K. Chanda, “Isotropic damage constitutive model for time-dependent behaviour of tunnels in squeezing ground,” *Comput. Geotech.*, vol. 127, p. 103738, 2020. <https://doi.org/10.1016/j.compgeo.2020.103738>
- [8] C. Ding, K. X. Xue, and C. H. Zhou, “Case study on long-term deformation monitoring and numerical simulation of layered rock slopes on both sides of Wudongde dam reservoir area,” *Sci. Rep.*, vol. 14, no. 1, p. 6909, 2024. <https://doi.org/10.1038/s41598-024-57598-7>
- [9] J. M. Wang, Z. H. Zhou, C. Chen, H. Wang, and Z. H. Chen, “Failure mechanism and stability analysis of an open-pit slope under excavation unloading conditions,” *Front. Earth Sci.*, vol. 11, pp. 1–11, 2023. <https://doi.org/10.3389/feart.2023.1109316>
- [10] X. Chen, J. L. Li, H. F. Deng, L. Dang, Q. Liu, X. X. Wang, and W. Wang, “Uncoordinated deformation of soft and hard interconnecting strata under unloading creep conditions,” *Rock Soil Mech.*, vol. 44, no. 1, 2023. <https://doi.org/10.16285/j.rsm.2022.0281>
- [11] C. Chen, L. P. Liu, and Y. Cong, “Experimental investigation on deformation and strength behavior of marble with the complex loading-unloading stress path,” *Adv. Civ. Eng.*, vol. 2020, p. 8853044, 2020. <https://doi.org/10.1155/2020/8853044>
- [12] Q. B. Meng, X. Zhang, S. L. Zhu, H. Pu, J. F. Liu, Y. L. Chen, and J. Y. Wu, “Experimental study on rock strength and deformation characteristics under triaxial cyclic loading and unloading conditions,” *Rock Mech. Rock Eng.*, vol. 310, p. 110529, 2021. <https://doi.org/10.1016/j.engfracmech.2024.110529>
- [13] J. Zhao, G. Guo, D. Xu, X. Huang, C. Hu, Y. Xia, and D. Zhang, “Experimental study of deformation and failure characteristics of deeply-buried hard rock under triaxial and cyclic loading and unloading stress paths,” *Rock Soil Mech.*, vol. 41, no. 5, pp. 1521–1530, 2020. <https://doi.org/10.16285/j.rsm.2019.1604>
- [14] J. Zhao and T. Zhang, “Experimental study on mechanical properties of deep buried granite under different confining pressures,” *Adv. Civ. Eng.*, vol. 2020, p. 6640497, 2020. <https://doi.org/10.1155/2020/6640497>
- [15] N. Y. Zhao and H. F. Jiang, “Mathematical methods to unloading creep constitutive model of rock mass under high stress and hydraulic pressure,” *Alex. Eng. J.*, vol. 60, no. 1, pp. 25–38, 2021. <https://doi.org/10.1016/j.aej.2020.04.033>
- [16] L. Yan, W. Xu, R. Wang, and W. C. Xie, “Mechanical and permeability characteristics of basalt during unloading confining pressure creep tests under coupled hydro-mechanical conditions,” *Rock Mech. Rock Eng.*, vol. 54, no. 12, pp. 6091–6103, 2021. <https://doi.org/10.1007/s00603-021-02616-7>
- [17] Q. Yan, S. F. Qin, X. F. Sang, Z. S. Luo, and M. H. Liang, “Research on creep characteristics of loading and unloading of hard Flint limestone,” *Front. Mater.*, vol. 10, pp. 1–12, 2023. <https://doi.org/10.3389/fmats.2023.1177733>
- [18] X. J. Zhang, J. Zhao, M. F. Jiang, J. C. Xue, and B. G. He, “Creep failure mechanism and model of granite under true triaxial loading and unloading conditions,” *Int. J. Geomech.*, vol. 24, no. 10, 2024. <https://doi.org/10.1061/ijgnai.Gmeng-9622>
- [19] S. S. Wang, W. Xu, H. Chen, and L. Yan, “The time-dependent behaviour and failure mechanism of dacite under unloading condition,” *Eur. J. Environ. Civ. Eng.*, vol. 26, no. 15, pp. 7756–7770, 2022. <https://doi.org/10.1080/19648189.2021.2009035>
- [20] C. Wang, J. Liu, L. Chen, J. Liu, and L. Wang, “Mechanical behaviour and damage evolution of beishan granite considering the transient and time-dependent effects of excavation unloading,” *Eur. J. Environ. Civ. Eng.*, vol. 26, no. 8, pp. 3187–3203, 2022. <https://doi.org/10.1080/19648189.2020.1784292>
- [21] G. H. Li, Y. T. Wang, D. Wang, X. X. Yang, L. G. Wang, Y. F. Li, and S. P. Zhang, “Creep damage model of rock with varying-parameter under the step loading and unloading conditions,” *Sci. Rep.*, vol. 11, no. 1, p. 24057, 2021. <https://doi.org/10.1038/s41598-021-03539-7>